Premature endocycling of *Drosophila* follicle cells causes pleiotropic defects in oogenesis

Hunter C. Herriage[1] and Brian R. Calvi[1,2]

1: Department of Biology, Indiana University, Bloomington, IN 47405

2: Corresponding author, bcalvi@indiana.edu

Keywords: endocycling, border cells, polyploidy, oogenesis, epithelium, *Drosophila*

Summary Statement

A premature switch to polyploid endocycles in *Drosophila* ovarian follicle cells caused pleiotropic defects in oogenesis and compromised female fertility, revealing new ways in which unscheduled endocycles cause developmental defects.

Abstract

Endocycling cells grow and repeatedly duplicate their genome without dividing. Cells switch from mitotic cycles to endocycles in response to developmental signals during the growth of specific tissues in a wide range of organisms. The purpose of switching to endocycles, however, remains unclear in many tissues. Additionally, cells can switch to endocycles in response to conditional signals, which can have beneficial or pathological effects on tissues. However, the impact of these unscheduled endocycles on development is underexplored. Here, we use *Drosophila* ovarian somatic follicle cells as a model to examine the impact of unscheduled endocycles on tissue growth and function. Follicle cells normally switch to endocycles at mid-oogenesis. Inducing follicle cells to prematurely switch to endocycles resulted in lethality of the resulting embryos. Analysis of ovaries with precocious follicle cell endocycles revealed aberrant follicular epithelial structure and pleiotropic defects in oocyte growth, developmental gene amplification, and the migration of a special set of follicle cells known as border cells. Overall, these findings reveal how unscheduled endocycles can disrupt tissue growth and function to cause aberrant development.

Introduction

Many tissues grow via the canonical mitotic division cycle while others grow via a variant cell cycle known as the endocycle. Endocycles are a cell cycle characterized by alternating G and S phases without mitotic division, with repeated endocycles resulting in the growth of large polyploid cells (Calvi, 2013). A regulated switch from mitotic cycles to endocycles is part of normal developmental growth programs of specific tissues across *Eukarya* (Fox and Duronio, 2013; Ovrebo and Edgar, 2018; Shu et al., 2018). We call these developmental endocycles. In contrast, cells can also switch to unscheduled endocycles in response to stress and other conditional signals, which we refer to as induced endocycling cells (Bailey et al., 2021; Hassel et al., 2014; Qi and Calvi, 2016; Rotelli et al., 2019). These induced endocycling cells can be beneficial for wound healing and regeneration, but they can also have pathological effects on tissue growth, including the promotion of cancer (Bailey et al., 2021; Herriage et al., 2023; Pienta et al., 2022; Shu et al., 2018). Much remains unknown, however, about why certain tissues switch to endocycles to support their growth, or how unscheduled endocycling affects tissue structure and function.

In this study we use the somatic follicle cells of the *Drosophila* ovary as a model to evaluate the effects of unscheduled endocycles on tissue function. A *Drosophila* ovary consists of ~16 ovarioles, each of which is composed of one stem cell compartment known as the germarium followed by an “assembly line” of progressively developing egg chambers in 14 stages of oogenesis (Fig. 1A) (Duhart et al., 2017; King, 1970). These developing egg chambers are composed of the germline (15 endocycling nurse cells and one oocyte) that is ensheathed by an epithelium of somatic follicle cells, whose cell cycle switches are coordinated with maturation of the egg chamber (Fig. 1A) (Jia et al., 2015; King, 1970). Follicle cells originate from a population of two to four somatic stem cells in the germarium and proliferate through mitotic cycles over the course of about three days until stage 6 of oogenesis, reaching numbers of approximately 650 follicle cells per egg chamber (Fadiga and Nystul, 2019; Margolis and Spradling, 1995; Sun and Deng, 2007). In response to Notch signaling at stages 6 / 7, follicle cells switch to the endocycle and subsequently complete three genome duplications over the next ~24 hours (Fig. 1A) (Calvi et al., 1998; Deng et al., 2001; Lopez-Schier and St Johnston, 2001; Spradling, 1993). After achieving a DNA copy number (C) of 16C, follicle cells arrest endocycles at different times (asynchronously) during late stage

9, but the mechanism of this cell autonomous arrest is unknown. Follicle cells then synchronously initiate a specialized DNA replication program known as chorion gene amplification at the onset of stage 10B (Fig. 1A) (Calvi et al., 1998). During chorion gene amplification, the genomic loci that encode eggshell proteins undergo repeated site-specific rereplication, and disruption of this gene amplification results in thin eggshells and embryonic lethality (Calvi, 2006; Spradling and Mahowald, 1980). Follicle cells also support egg growth by mediating transport of yolk proteins into the oocyte and participate in patterning of the egg and embryo (Brennan et al., 1982; Duhart et al., 2017; Merkle et al., 2020; Raikhel and Dhadialla, 1992). While it is known that follicle cells have these important roles in oogenesis, it remains unclear what biological function is served by the endocycle switch occurring specifically at stage 6.

We have previously shown that follicle cells in both developmental and experimentally induced endocycles repress the apoptotic response to DNA damage (Hassel et al., 2014; Mehrotra et al., 2008; Qi and Calvi, 2016). In this study, we find that a precocious switch to the endocycle results in pleiotropic defects in the structure and function of the follicular epithelium and severely compromised female fertility. Overall, our data show that unscheduled endocycles can have severe negative consequences, with broader impacts on understanding how they may contribute to human developmental abnormalities and disease.

Results and Discussion

Induction of precocious endocycles in follicle cells

To address whether a switch to follicle cell endocycles before stage 6 would affect oogenesis, we induced precocious endocycling by expressing the protein Roughex (Rux), a known repressor of Cyclin A / CDK1 activity and mitotic entry (Avedisov et al., 2000; Sprenger et al., 1997). A *tj-GAL4* transgene was used to induce expression of a *UAS-Roughex* (*UAS-Rux*) transgene in all ovarian somatic cells, and a temperature-sensitive GAL80^{ts} repressor of GAL4 permitted control over the timing of expression (Brand and Perrimon, 1993; McGuire et al., 2004; Weaver et al., 2020). The *tj-GAL4 tub-GAL80^{ts} / UAS-Rux* experimental and *tj-GAL4 tub-GAL80^{ts} /* + control animals without *UAS-Rux* were raised at 18°C to repress GAL4 activity. Adult flies were then shifted to 29°C to induce *UAS-Rux* expression and ovaries were examined one and two days thereafter (Fig. 1A). Within one day after *UAS-Rux* expression, stage 1-6 follicle cells ceased labeling for the mitotic marker phosphorylated Histone H3 (pH3),

96 but continued to incorporate the nucleotide analog 5-ethynyl 2′-deoxyuridine (EdU), suggesting
97 that they had switched to G / S endocycles (Fig. S1 A-D′).
98 We next asked what effect precocious endocycle induction would have on follicle cells
99 as they matured to later stages of oogenesis (Fig. 1A). Two days after a shift to 29°C, stage
100 10B egg chambers from control females had a normal ~641 follicle cells, and measurement of
101 DAPI fluorescence indicated that they had the normal average DNA content of ~16C (Fig. 1 A-
102 B′, D, E) (Calvi et al., 1998; Sun and Deng, 2007). In contrast, induction of precocious
103 endocycles two days earlier resulted in stage 10B egg chambers that had four-fold fewer
104 follicle cells (~179) and nearly a four-fold increase in average DNA content (mean ploidy ~56
105 C) (Fig. 1 C-E). Immunolabeling for E-cadherin also indicated that these stage 10B follicle cells
106 were larger than normal, consistent with the known scaling of cell size with DNA ploidy (Fig.
107 1B′, C′) (Cadart and Heald, 2022; Tepass et al., 1996; Uemura et al., 1996). These results
108 suggest that Rux-expressing follicle cells had skipped two mitotic divisions and instead
109 underwent two extra genome doublings during endocycles. These results are consistent with
110 the known rate of oogenesis at 29°C (Gandara and Drummond-Barbosa, 2022). These stage
111 10B egg chambers would have been in approximately stage 4 / 5 two days earlier at the time
112 of temperature shift (Gandara and Drummond-Barbosa, 2022). In wild type, follicle cells in a
113 stage 4 / 5 egg chamber undergo an average of two mitotic divisions over one day as it
114 matures to stage 6 / 7, after which follicle cells endocycle over the next day from stage 7 to
115 stage 10A (Calvi et al., 1998; Margolis and Spradling, 1995). Given that there were two extra
116 endocycles instead of the normal two mitotic divisions during the ~24 hours from stage 4 / 5 to
117 stage 6 / 7, these data also suggest that the duration of each induced endocycle is
118 approximately equal to that of the normal mitotic cycles that they supplanted (Margolis and
119 Spradling, 1995). Moreover, the increased DNA content of these follicle cells at stage 10
120 suggests that starting endocycles early can override the undefined mechanisms that normally
121 limit follicle cell ploidy to 16C.
122
123 <u>Precocious endocycling has deleterious effects on egg quality and female fertility</u>
124 We next examined whether precocious follicle cell endocycles affected the morphology
125 of late-stage egg chambers. Stage 10B egg chambers from Rux-expressing females appeared
126 similar to those from controls (Fig 1B-C’). The main body follicle cells underwent normal
127 migration posteriorly during stage 9 to over the growing oocyte (Figs. 1B-C’, 2A-D).

128 Measurements indicated that one day after temperature shift, stage 10B egg chambers from
129 Rux-expressing females had oocytes of a similar size to controls (Fig. 2A- E). These egg
130 chambers would have been in approximately stage 6 / 7 one day earlier at the time of
131 temperature shift, a stage when follicle cells normally enter endocycles, and, therefore, would
132 have begun endocycles no more than a few hours earlier than controls. Conversely, two days
133 after temperature shift, the Rux-expressing stage 10B egg chambers that had begun
134 endocycles in stage 4 / 5 had oocytes that were smaller than controls (Fig. 2C-E).
135 Correspondingly, the length of the nurse cell compartment in these stage 10B egg chambers
136 was larger than controls after two days of Rux expression (Fig. 2F). These results suggest that
137 the two extra follicle cell endocycles have non-autonomous effects on germline growth, which
138 may include the normal function of follicle cells to mediate oocyte yolk deposition (Brennan et
139 al., 1982; Horne-Badovinac and Bilder, 2005; Isasti-Sanchez et al., 2021; Raikhel and
140 Dhadialla, 1992).

141 Another important function of follicle cells is to synthesize the eggshell late in
142 oogenesis, a process that is supported by chorion gene amplification (Fig. 1A) (Calvi et al.,
143 1998; Spradling and Mahowald, 1980). This selective developmental gene amplification can be
144 detected as distinct foci of EdU incorporation beginning in stage 10B (Calvi et al., 1998). EdU
145 labeling of *tj-GAL4 GAL80^{ts} /* + control ovaries at 29°C showed that all follicle cells over the
146 oocyte had nuclear foci of EdU at the onset of stage 10B, indicating that the onset of
147 amplification was synchronized among follicle cells, as previously described for wild type (Fig.
148 2G, I-I′, K) (Calvi et al., 1998). Follicle cells that had been expressing Rux for 24 hours also
149 had the normal transition to synchronous amplification in stage 10B (Fig. 2H). In contrast,
150 induction of precocious endocycles two days earlier resulted in some stage 10B egg chambers
151 with a mixture of follicle cells, with some having the normal amplification foci while others had
152 pan-nuclear EdU incorporation indicative of continued genomic replication (Fig. 2J-K). These
153 results suggest that premature endocycles in earlier oogenesis disrupt the normal cessation of
154 endocycles and the synchronous transition of follicle cells into amplification in later oogenesis.

155 Defects in chorion gene amplification are known to result in thin eggshells and reduced
156 embryo viability (Calvi, 2006). We therefore examined whether precocious endocycles
157 impaired eggshell synthesis. Females expressing *UAS-Rux* began laying eggs with thin shells
158 beginning one day after induction, a phenotype that greatly increased in frequency after two
159 days, with almost all laid eggs having thin shells by three days (Fig. 2L-P, Fig. S2A, B).

160 Expression of Rux in females also resulted in reduced viability of their embryos, as evidenced
161 by a reduction in egg hatching beginning on day one, which was further reduced on days two
162 and three (Fig. 2Q). Three or more days of Rux expression resulted in ovarioles with
163 degenerating stage 8-9 egg chambers, which is diagnostic of an ovarian stress response
164 known as the vitellogenic checkpoint (Fig. S2 C, D) (McCall, 2004; Peterson et al., 2015;
165 Serizier and McCall, 2017). These degenerating stage 8 egg chambers would have been in
166 stage 1 / 2 three days earlier at the time of induction, which suggests that very early entry into
167 endocycles triggers a general stress response. All together, these data indicate that induction
168 of precocious follicle cell endocycles has deleterious effects on egg quality and female fertility.
169

170 <u>Precocious endocycles cause structural defects in the follicular epithelium</u>

171 Our observations that there was a one to several day delay in oogenesis defects and
172 reduced embryo viability after Rux expression suggested that these defects were the
173 manifestation of precocious endocycle entry at earlier stages. To investigate early stage egg
174 chamber morphology, we examined the effects of precocious endocycles on the follicular
175 epithelium of early-stage egg chambers by immunolabeling for the cell-cell junction structural
176 protein E-cadherin and DAPI staining (Godt and Tepass, 1998; Oda et al., 1997; Tepass et al.,
177 1996; Uemura et al., 1996). Although EdU and pH3 labeling had indicated that follicle cells
178 switch to endocycles within one day of Rux expression, this duration of induced endocycling
179 did not result in major defects in epithelial structure (Figs. S1A-B′, 3A-B″). These follicle cells
180 had normal, uniform, cuboidal structure and E-cadherin labeling on their apical surface that is
181 adjacent to the germline (Fig. 3A-B″) (Godt and Tepass, 1998; Gonzalez-Reyes and St
182 Johnston, 1998). In contrast, after two days of Rux expression, follicle cells were larger with
183 wide variations in both their size and shape within an egg chamber (Fig. 3C-D″). Some follicle
184 cells had highly irregular shapes, with different parts of the cell having unequal thicknesses in
185 the apical / basal axis, and many with highly irregular E-cadherin labeling (Fig. 3D-D″). In
186 confocal sections through the middle of egg chambers, the interface between the follicular
187 epithelium and germline appeared wavy instead of the normal smooth circular interface,
188 suggesting global deformations of tissue morphology (Fig. 3C′, D′). Labeling for the
189 membrane-associated protein Discs large 1 (Dlg1) also revealed irregular cell sizes and
190 shapes, but Dlg1 had an overall normal basolateral localization, suggesting that there was not
191 a severe disruption of cell polarity (Fig. S3 A-D″) (Khoury and Bilder, 2020; Woods et al.,

192 1996). All follicle cells in these aberrant egg chambers had an increased DNA content
193 consistent with having proceeded through one to several precocious endocycles (Fig. 3C-E).
194 The correlation of these epithelial phenotypes with polyploidy suggests that precocious
195 endocycles have detrimental effects on follicle cell shape, epithelial structure, and egg
196 chamber morphology. These disruptions of epithelial structure in early stages may contribute to
197 the activation of the vitellogenic checkpoint and the observed defects in the transition to
198 amplification as egg chambers mature into later stages over subsequent days.
199

200 Precocious endocycling inhibits border cell migration

201 Unlike the main body follicle cells that migrate on the surface of the egg chamber,
202 another group of follicle cells delaminate from the anterior epithelium and migrate posteriorly
203 between the nurse cells during stage 9 (Mishra et al., 2019; Montell et al., 1992; Montell et al.,
204 2012; Spradling, 1993). This collective migration event is initiated in early stage 9 when two
205 specialized follicle cells, known as the polar cells, recruit 4-6 neighboring follicle cells to
206 become border cells via JAK-STAT signaling (Montell et al., 1992; Silver and Montell, 2001).
207 After arriving at their final destination at the anterior of the growing oocyte in stage 10A, this
208 migrating border cell cluster forms the sperm entry port known as the micropyle (Bishop and
209 King, 1984; King, 1970). Because these border cells have been a powerful model for cellular
210 and molecular mechanisms of collective cell migration during development and cancer
211 metastasis, we wished to investigate the effect of precocious endocycling on their migration.

212 We identified border cells based on their elevated E-cadherin levels in control and Rux-
213 expressing ovaries two days after induction at 29°C and measured the distance they had
214 migrated relative to main body follicle cells in the same egg chamber during stage 9-10A
215 (Niewiadomska et al., 1999; Oda et al., 1997). In controls, the migration of the border cell
216 cluster between the nurse cells stays on-pace with the anterior of the main body follicle cells
217 that are migrating on the surface of the egg chamber during stage 9, with both populations of
218 follicle cells reaching the oocyte at the onset of stage 10A (Fig. 4A, A', C) (Horne-Badovinac
219 and Bilder, 2005; Montell et al., 1992; Silver et al., 2005). In contrast, Rux expression resulted
220 in border cells lagging behind the main body follicle cells to varying extents (Fig. 4B-C). In
221 some egg chambers, border cells had failed to even delaminate from the epithelium at the
222 anterior pole of the egg chamber by stage 10 (Fig. 4C).

223 Having abnormal numbers of polar cells or border cells can inhibit border cell cluster
224 delamination and migration (Silver et al., 2005; Silver and Montell, 2001). Labeling for the polar
225 cell marker protein Fasciclin III (Fas III) showed that after two days of Rux expression egg
226 chambers had the normal two polar cells, including those in which border cells migrated slowly
227 or failed to delaminate from the epithelium (Fig. 4D-E‴) (Ruohola et al., 1991). Co-labeling
228 against E-cadherin indicated that these migrating clusters had normal structure and cell
229 polarity (Fig. 4 D-E‴). While some Rux-expressing egg chambers had a reduced number of
230 cells per cluster, even clusters composed of the normal two polar cells and four to six border
231 cells were delayed in their migration (Fig. 4 B, B′, E-E‴). Previous reports had indicated that
232 polyploidy enhanced the migration of cancer cells *in vitro*, leading to suggestions that
233 polyploidy may promote metastasis *in vivo* (Godinho et al., 2014; Mallin et al., 2023; Wang et
234 al., 2019). Our results modify that view and suggest that unscheduled endocycles can also
235 inhibit cellular migration in some contexts.
236
237 Conclusions
238 We have found that premature follicle cell endocycles cause pleiotropic defects in
239 oogenesis and severely compromise female fertility. Although follicle cells normally undergo a
240 cell-autonomous endocycle arrest at 16C DNA content during stage 9, starting endocycles
241 early resulted in a >16C DNA content by stage 10. This suggests that either there is not a DNA
242 counting mechanism that induces endocycle arrest, or that starting endocycles early bypassed
243 that mechanism. Moreover, some of these cells continued genome duplications into later
244 stages of oogenesis, which further increased their ploidy and disrupted the transition to chorion
245 gene amplification, and also resulted in thin eggshells. Several proteins have been implicated
246 in the transition from endocycles to the chorion gene amplification phase, but molecular
247 mechanisms remain incompletely defined (Calvi, 2006; Huang et al., 2013; Sun et al., 2008).
248 Further analysis of these induced endocycles may provide insight into the mechanisms that
249 coordinate the timely transition from endocycles to amplification during stage 10, which may
250 also govern endocycle arrest and final DNA content in other cell types.
251 Premature endocycles disrupted cell and epithelial morphology, which may be related
252 to the observed reduction in oocyte growth in stage 10 egg chambers. Follicle cells mediate
253 the growth and nutritive content of the oocyte by mediating the deposition of yolk protein into
254 the oocyte beginning in stage 8. The majority of yolk protein is made in the fat body and

transported around follicle cells via a paracellular transport process that is enabled by a regulated increase in epithelial permeability, a state known as patency (Isasti-Sanchez et al., 2021; Riechmann, 2021). Patency involves remodeling of cell-cell junctions through a mechanism that includes E-cadherin, whose labeling was altered in precocious endocycling follicle cells (Horne-Badovinac and Bilder, 2005; Isasti-Sanchez et al., 2021). Thus, the aberrant cell and epithelial morphology we observe in induced endocycling cells may disturb the remodeling of cell-cell contacts that is required for patency and oocyte growth. More broadly, these results suggest that disrupted epithelial structure and permeability in other tissues may be another way for unscheduled endocycles to contribute to disease.

Precocious endocycles strongly inhibited border cell delamination and migration, but further investigation is necessary to define the links between unscheduled endocycles and migration. Our observation of impaired collective border cell migration contrasts with recent evidence that polyploidy enhances migration of cancer cells *in vitro,* and suggestions that it promotes collective cell migration during metastasis (Godinho et al., 2014; Mallin et al., 2023; Wang et al., 2019). It remains possible, however, that the effects of unscheduled endocycles on cell migration are dependent on cell type and tissue context. In addition, oncogenic mutations may synergize with the polyploid state to give rise to emergent migratory properties (Almeida Machado Costa et al., 2022).

Overall, our findings show that unscheduled endocycles can have severe pleiotropic effects on tissue growth and function. Further characterization of these effects will lead to a greater understanding of how endocycling, both scheduled and unscheduled, can influence tissue growth and contribute to disease.

278 **Materials and Methods**

279 *Drosophila* genetics: Crosses of *tj-GAL4 tub-GAL80^{ts} / CyO* to *w^{1118}* (control) or *UAS-Rux /*
280 *SM6a* (experimental) were conducted, and their offspring were reared, at 18°C during larval
281 and early adult development. The resulting adult female offspring were fed wet yeast with
282 males for 2 days at 18°C before being transferred to new wet yeast and shifted to 29°C for 1,
283 2, or 3 days (as noted in the text). The females and males were transferred to new wet yeast
284 every 2 days during the experiments. The *tj-GAL4, tub-GAL80^{ts}* / *CyO* strain was a generous
285 gift from L. Weaver. The *UAS-Rux / SM6a* strain was obtained from the Bloomington
286 Drosophila Stock Center (BDSC #9166).

287

288 Immunofluorescence microscopy: Ovaries were fixed and labeled as previously described
289 (Schwed et al., 2002). For E-cadherin labeling, fixation buffers were supplemented with 1 mM
290 $CaCl_2$. The following antibodies and dilutions were used: rat anti-shg (fly E-cadherin), 1:20
291 (DSHB DCAD2); rabbit anti-phosphorylated histone H3 (pH3), 1:1000 (Millipore 06-570);
292 mouse anti-Dlg1, 1:200 (DSHB 4F3); mouse anti-FasIII, 1:50 (DSHB 7G10). EdU incorporation
293 *in vitro* was for 1 hour as previously described (Calvi and Lilly, 2004). Asynchronous chorion
294 gene amplification was defined by stage 10B egg chambers with both punctate and pan-
295 nuclear EdU labeling of follicle cell nuclei. Egg chambers with more than one pan-nuclear EdU
296 labeled nucleus were scored as "asynchronous." Fluorescence micrographs were taken on a
297 Leica SP8 confocal. DIC images of stage 10B egg chambers were taken using a Leica
298 DM5500 B. Brightfield images of laid eggs were taken using a Zeiss SteREO Discovery.V12.
299 Nuclear DNA content was quantified using ImageJ/FIJI by measuring mean DAPI fluorescence
300 per pixel in a nucleus, subtracting local mean background DAPI fluorescence per pixel, and
301 then multiplying the difference by the number of pixels per nucleus to obtain the corrected total
302 DAPI fluorescence intensity. The number of follicle cells, oocyte area, nurse cell compartment
303 length, and border cell migration were quantified using ImageJ/FIJI.

304

305 Eggshell scoring and egg hatch rate: Eggs from well-fed and mated females were collected on
306 grape plates with a thin layer of yeast paste for 2-4 hours for each respective day of 29°C
307 transgene induction. After counting the number of eggs with thin eggshells, eggs were lined up

308 and incubated at 18°C to ensure no GAL4-driven transgene expression affected their viability.
309 They were then scored for hatching over four subsequent days.

310

311 Statistical Analysis: Data graphing and statistical analyses were carried out in GraphPad
312 Prism. Data were tested for normality and homoscedasticity to determine correct analyses.
313 Sample size (n) is defined as the total of independent observations / measurements used for
314 the chosen analysis across multiple biological replicates. All averages shown are mean ± s.d.,
315 except for Figure 2K, which is mean ± s.e.m. Two-tailed Mann-Whitney tests were used to test
316 for significance in Figs. 1D, 2E, and 3E. Fig. 2E was corrected for multiple comparisons. A two-
317 tailed unpaired Welch's t-test was used to test for significance in Fig. 1E. A Mixed Effects Two-
318 Way ANOVA was used to test for significance in Fig. 2F. A two-tailed unpaired t-test was used
319 to test for significance in Fig. 2K.

320

Acknowledgements

We thank S. Brown and Y.T. Huang for experimental assistance. We are appreciative of the thoughtful feedback on the research and manuscript from S. Brown, L. Hesting, Y.T. Huang, P. Rangarajan, and C. Walczak. We thank A. Kun and J. Powers of the IU Light Microscopy Imaging Center, supported in part by the Office of the Vice Provost of Research. Special thanks to L. Weaver for her generous gift of the *tj-GAL4 tub-GAL80^{ts} / CyO* strain.

Competing Interests

The authors declare no competing interests.

Author Contributions

H.C.H. performed experiments and statistical analyses. Both authors wrote and edited the manuscript. B.R.C. secured funding and provided mentorship and supervision.

Funding

This work was supported by National Institutes of Health Grant NIH R01GM113107 to B.R.C.

References

Almeida Machado Costa, C., Wang, X. F., Ellsworth, C. and Deng, W. M. (2022). Polyploidy in development and tumor models in Drosophila. *Semin Cancer Biol* **81**, 106-118.

Avedisov, S. N., Krasnoselskaya, I., Mortin, M. and Thomas, B. J. (2000). Roughex mediates G(1) arrest through a physical association with cyclin A. *Mol Cell Biol* **20**, 8220-8229.

Bailey, E. C., Kobielski, S., Park, J. and Losick, V. P. (2021). Polyploidy in Tissue Repair and Regeneration. *Cold Spring Harb Perspect Biol* **13**.

Bishop, D. L. and King, R. C. (1984). An ultrastructural study of ovarian development in the otu-7 mutant of Drosophila melanogaster. *J. Cell Sci.* **67**, 87-119.

Brand, A. and Perrimon, N. (1993). Targeted gene expression as a means of altering cell fates and generating dominant phenotypes. *Development* **118**, 401-415.

Brennan, M. D., Weiner, A. J., Goralski, T. J. and Mahowald, A. P. (1982). The follicle cells are a major site of vitellogenin synthesis in Drosophila melanogaster. *Dev Biol* **89**, 225-236.

Cadart, C. and Heald, R. (2022). Scaling of biosynthesis and metabolism with cell size. *Molecular Biology of the Cell* **33**, pe5.

Calvi, B. R. (2006). Developmental DNA amplification. In *DNA replication and human disease* (ed. M. L. DePamphilis), pp. 233-255. Cold Spring Harbor, NY: Cold Spring Harbor Laboratory Press.

Calvi, B. R. (2013). Making big cells: one size does not fit all. *Proc Natl Acad Sci U S A* **110**, 9621-9622.

Calvi, B. R., Lilly, M. A. and Spradling, A. C. (1998). Cell cycle control of chorion gene amplification. *Genes Dev* **12**, 734-744.

Deng, W. M., Althauser, C. and Ruohola-Baker, H. (2001). Notch-Delta signaling induces a transition from mitotic cell cycle to endocycle in Drosophila follicle cells. *Development* **128**, 4737-4746.

Duhart, J. C., Parsons, T. T. and Raftery, L. A. (2017). The repertoire of epithelial morphogenesis on display: Progressive elaboration of Drosophila egg structure. *Mech Dev* **148**, 18-39.

Fadiga, J. and Nystul, T. G. (2019). The follicle epithelium in the Drosophila ovary is maintained by a small number of stem cells. *Elife* **8**.

Fox, D. T. and Duronio, R. J. (2013). Endoreplication and polyploidy: insights into development and disease. *Development* **140**, 3-12.

Gandara, A. C. P. and Drummond-Barbosa, D. (2022). Warm and cold temperatures have distinct germline stem cell lineage effects during Drosophila oogenesis. *Development* **149**.

Godinho, S. A., Picone, R., Burute, M., Dagher, R., Su, Y., Leung, C. T., Polyak, K., Brugge, J. S., Thery, M. and Pellman, D. (2014). Oncogene-like induction of cellular invasion from centrosome amplification. *Nature* **510**, 167-171.

Godt, D. and Tepass, U. (1998). Drosophila oocyte localization is mediated by differential cadherin-based adhesion. *Nature* **395**, 387-391.

Gonzalez-Reyes, A. and St Johnston, D. (1998). The Drosophila AP axis is polarised by the cadherin-mediated positioning of the oocyte. *Development* **125**, 3635-3644.

Hassel, C., Zhang, B., Dixon, M. and Calvi, B. R. (2014). Induction of endocycles represses apoptosis independently of differentiation and predisposes cells to genome instability. *Development* **141**, 112-123.

Herriage, H. C., Huang, Y. T. and Calvi, B. R. (2023). The antagonistic relationship between apoptosis and polyploidy in development and cancer. *Semin Cell Dev Biol*.

Horne-Badovinac, S. and Bilder, D. (2005). Mass transit: epithelial morphogenesis in the Drosophila egg chamber. *Dev Dyn* **232**, 559-574.

Huang, Y. C., Smith, L., Poulton, J. and Deng, W. M. (2013). The microRNA miR-7 regulates Tramtrack69 in a developmental switch in Drosophila follicle cells. *Development* **140**, 897-905.

Isasti-Sanchez, J., Munz-Zeise, F., Lancino, M. and Luschnig, S. (2021). Transient opening of tricellular vertices controls paracellular transport through the follicle epithelium during Drosophila oogenesis. *Dev Cell* **56**, 1083-1099 e1085.

Jia, D., Huang, Y. C. and Deng, W. M. (2015). Analysis of Cell Cycle Switches in Drosophila Oogenesis. *Methods Mol Biol* **1328**, 207-216.

Khoury, M. J. and Bilder, D. (2020). Distinct activities of Scrib module proteins organize epithelial polarity. *Proc Natl Acad Sci U S A* **117**, 11531-11540.

King, R. C. (1970). *Ovarian Development in Drosophila melanogaster*. New York: Academic Press.

Lopez-Schier, H. and St Johnston, D. (2001). Delta signaling from the germ line controls the proliferation and differentiation of the somatic follicle cells during Drosophila oogenesis. *Genes Dev* **15**, 1393-1405.

Mallin, M. M., Kim, N., Choudhury, M. I., Lee, S. J., An, S. S., Sun, S. X., Konstantopoulos, K., Pienta, K. J. and Amend, S. R. (2023). Cells in the polyaneuploid cancer cell (PACC) state have increased metastatic potential. *Clin Exp Metastasis* **40**, 321-338.

Margolis, J. and Spradling, A. (1995). Identification and behavior of epithelial stem cells in the Drosophila ovary. *Development* **121**, 3797-3807.

McCall, K. (2004). Eggs over easy: cell death in the Drosophila ovary. *Dev Biol* **274**, 3-14.

McGuire, S. E., Mao, Z. and Davis, R. L. (2004). Spatiotemporal gene expression targeting with the TARGET and gene-switch systems in Drosophila. *Sci STKE* **2004**, pl6.

Mehrotra, S., Maqbool, S. B., Kolpakas, A., Murnen, K. and Calvi, B. R. (2008). Endocycling cells do not apoptose in response to DNA rereplication genotoxic stress. *Genes Dev* **22**, 3158-3171.

Merkle, J. A., Wittes, J. and Schupbach, T. (2020). Signaling between somatic follicle cells and the germline patterns the egg and embryo of Drosophila. *Curr Top Dev Biol* **140**, 55-86.

Mishra, A. K., Campanale, J. P., Mondo, J. A. and Montell, D. J. (2019). Cell interactions in collective cell migration. *Development* **146**.

Montell, D. J., Rorth, P. and Spradling, A. C. (1992). slow border cells, a locus required for a developmentally regulated cell migration during oogenesis, encodes Drosophila C/EBP. *Cell* **71**, 51-62.

Montell, D. J., Yoon, W. H. and Starz-Gaiano, M. (2012). Group choreography: mechanisms orchestrating the collective movement of border cells. *Nat Rev Mol Cell Biol* **13**, 631-645.

Niewiadomska, P., Godt, D. and Tepass, U. (1999). DE-Cadherin is required for intercellular motility during Drosophila oogenesis. *J Cell Biol* **144**, 533-547.

429 **Oda, H., Uemura, T. and Takeichi, M.** (1997). Phenotypic analysis of null mutants for DE-
430 cadherin and Armadillo in Drosophila ovaries reveals distinct aspects of their functions
431 in cell adhesion and cytoskeletal organization. *Genes Cells* **2**, 29-40.
432 **Ovrebo, J. I. and Edgar, B. A.** (2018). Polyploidy in tissue homeostasis and regeneration.
433 *Development* **145**.
434 **Peterson, J. S., Timmons, A. K., Mondragon, A. A. and McCall, K.** (2015). The End of the
435 Beginning: Cell Death in the Germline. *Curr Top Dev Biol* **114**, 93-119.
436 **Pienta, K. J., Hammarlund, E. U., Austin, R. H., Axelrod, R., Brown, J. S. and Amend, S.**
437 **R.** (2022). Cancer cells employ an evolutionarily conserved polyploidization program to
438 resist therapy. *Semin Cancer Biol* **81**, 145-159.
439 **Qi, S. and Calvi, B. R.** (2016). Different cell cycle modifications repress apoptosis at different
440 steps independent of developmental signaling in Drosophila. *Mol Biol Cell* **27**, 1885-
441 1897.
442 **Raikhel, A. S. and Dhadialla, T. S.** (1992). Accumulation of yolk proteins in insect oocytes.
443 *Annu Rev Entomol* **37**, 217-251.
444 **Riechmann, V.** (2021). Paracellular transport: Opening the gates for growth. *Dev Cell* **56**,
445 1075-1077.
446 **Rotelli, M. D., Policastro, R. A., Bolling, A. M., Killion, A. W., Weinberg, A. J., Dixon, M. J.,**
447 **Zentner, G. E., Walczak, C. E., Lilly, M. A. and Calvi, B. R.** (2019). A Cyclin A-Myb-
448 MuvB-Aurora B network regulates the choice between mitotic cycles and polyploid
449 endoreplication cycles. *PLoS Genet* **15**, e1008253.
450 **Ruohola, H., Bremer, K., Baker, D., Swedlow, J., Jan, L. and Jan, Y.** (1991). Role of
451 neurogenic genes in establishment of follicle cell fate and oocyte polarity during
452 oogenesis in Drosophila. *Cell* **66**, 433-449.
453 **Schwed, G., May, N., Pechersky, Y. and Calvi, B. R.** (2002). Drosophila minichromosome
454 maintenance 6 is required for chorion gene amplification and genomic replication. *Mol*
455 *Biol Cell* **13**, 607-620.
456 **Serizier, S. B. and McCall, K.** (2017). Scrambled Eggs: Apoptotic Cell Clearance by Non-
457 Professional Phagocytes in the Drosophila Ovary. *Front Immunol* **8**, 1642.
458 **Shu, Z., Row, S. and Deng, W. M.** (2018). Endoreplication: The Good, the Bad, and the Ugly.
459 *Trends Cell Biol* **28**, 465-474.
460 **Silver, D. L., Geisbrecht, E. R. and Montell, D. J.** (2005). Requirement for JAK/STAT
461 signaling throughout border cell migration in Drosophila. *Development* **132**, 3483-3492.
462 **Silver, D. L. and Montell, D. J.** (2001). Paracrine signaling through the JAK/STAT pathway
463 activates invasive behavior of ovarian epithelial cells in Drosophila. *Cell* **107**, 831-841.
464 **Spradling, A. and Mahowald, A.** (1980). Amplification of genes for chorion proteins during
465 oogenesis in Drosophila melanogaster. *Proc Natl Acad Sci U S A* **77**, 1096-1100.
466 **Spradling, A. C.** (1993). Developmental Genetics of Oogenesis. In *The Development of*
467 *Drosophila melanogaster* (ed. M. B. a. A. Martinez-Arias). Cold Spring Harbor, New
468 York: Cold Spring Harbor Press.
469 **Sprenger, F., Yakubovich, N. and O'Farrell, P. H.** (1997). S-phase function of Drosophila
470 cyclin A and its downregulation in G1 phase. *Curr Biol* **7**, 488-499.
471 **Sun, J. and Deng, W. M.** (2007). Hindsight mediates the role of notch in suppressing
472 hedgehog signaling and cell proliferation. *Dev Cell* **12**, 431-442.
473 **Sun, J., Smith, L., Armento, A. and Deng, W. M.** (2008). Regulation of the endocycle/gene
474 amplification switch by Notch and ecdysone signaling. *J Cell Biol* **182**, 885-896.

Tepass, U., Gruszynski-DeFeo, E., Haag, T. A., Omatyar, L., Torok, T. and Hartenstein, V. (1996). shotgun encodes Drosophila E-cadherin and is preferentially required during cell rearrangement in the neurectoderm and other morphogenetically active epithelia. *Genes Dev* **10**, 672-685.

Uemura, T., Oda, H., Kraut, R., Hayashi, S., Kotaoka, Y. and Takeichi, M. (1996). Zygotic Drosophila E-cadherin expression is required for processes of dynamic epithelial cell rearrangement in the Drosophila embryo. *Genes Dev* **10**, 659-671.

Wang, X., Zheng, M., Fei, F., Li, C., Du, J., Liu, K., Li, Y. and Zhang, S. (2019). EMT-related protein expression in polyploid giant cancer cells and their daughter cells with different passages after triptolide treatment. *Med Oncol* **36**, 82.

Weaver, L. N., Ma, T. and Drummond-Barbosa, D. (2020). Analysis of Gal4 Expression Patterns in Adult Drosophila Females. *G3 (Bethesda)* **10**, 4147-4158.

Woods, D. F., Hough, C., Peel, D., Callaini, G. and Bryant, P. J. (1996). Dlg protein is required for junction structure, cell polarity, and proliferation control in Drosophila epithelia. *J Cell Biol* **134**, 1469-1482.

492 **Figure Legends**

493 **Figure 1: Induction of precocious follicle cell endocycles.** (A) Drawing of a single ovariole
494 with select stages of oogenesis and follicle cell cycle transitions indicated below. Follicle cells
495 are colored pink. Above is the experimental timeline in relationship to the timing of egg
496 chamber maturation. (B-C′) DAPI staining and immunolabeling against E-cadherin in control
497 (B, B′) and Rux-expressing stage 10B egg chambers (C, C′); scale bar = 30 μm. (D)
498 Quantification of DNA Content in control and Rux-expressing stage 10B egg chambers.; **** p
499 < 0.0001; n = 85 nuclei in control and n = 104 nuclei in *UAS-Rux* across four biological
500 replicates. (E) Quantification of number of DAPI-labeled nuclei in control and Rux-expressing
501 stage 10B egg chambers; **** p < 0.0001; n = 12 egg chambers in both conditions across four
502 biological replicates.

503 **Figure 2: Precocious endocycling compromises egg quality and female fertility.** (A-D)
504 Differential interference contrast images of control (A, C) and Rux-expressing (B, D) stage 10B
505 egg chambers after one (A, B) or two (C, D) days of incubation at 29 °C; scale bar = 100 μm.
506 (E) Quantification of oocyte area in control and Rux-expressing stage 10 egg chambers.; * p <
507 0.05; for day one, n = 13 oocytes for control and n = 15 oocytes for UAS-*Rux* across three
508 biological replicates; for day 2, n = 20 oocytes for control and n=24 oocytes for UAS-*Rux*
509 across five biological replicates. (F) Quantification of nurse cell compartment length; ** p =
510 0.0021, *** p = 0.0002, **** p < 0.0001. For day 1, n = 20 egg chambers for control and UAS-
511 *Rux* across three biological replicates; for day 2, n = 27 egg chambers for control and n = 30
512 egg chambers for *UAS-Rux* across five biological replicates. (G-J′) DAPI staining and EdU
513 labeling of DNA replication in control (G, I, I′) and Rux-expressing (H, J, J′) stage 10B egg
514 chambers after one (G, H) or two (I-J′) days of incubation at 29 °C; scale bar = 25 μm (G-I, J)
515 or 10 μm (I′, J′). (K) Quantification of percent egg chambers that had chorion gene
516 amplification asynchrony in control and Rux-expressing ovaries. *** p = 0.0003; n = 26 egg
517 chambers for control; n = 19 egg chambers for *UAS-Rux* both across three biological
518 replicates. (L-O) Brightfield images of eggs laid by control (L, N) and Rux-expressing females
519 (M, O) after one (L, M) or two (N, O) days of incubation at 29 °C; scale bar = 200 μm.
520 Quantification of percent of eggs with thin shells (P) and hatch rate (Q) across three biological
521 replicates.

522

523 **Figure 3: Precocious endocycling disrupts follicular epithelial structure.** (A-D″) DAPI
524 staining and immunolabeling against E-cadherin in control (A-A″, C-C″) or Rux-expressing (B-
525 B″, D-D″) early-stage egg chambers after one (A-B″) or two (C-D″) days of incubation at 29 °C;
526 scale bar = 15 μm (A-D″). Stages of oogenesis (S) and germarium (G) are indicated. (E)
527 Quantification of DNA Content in control and Rux-expressing stage 4 / 5 egg chambers after
528 two days of incubation at 29°C.; **** $p < 0.0001$; n = 25 nuclei for control; n = 15 nuclei for
529 *UAS-Rux* both across three biological replicates.

530 **Figure 4: Precocious endocycling inhibits border cell migration.** (A-B′) DAPI staining and
531 immunolabeling against E-cadherin in control (A, A′) and Rux-expressing (B, B′) stage 10 egg
532 chambers after two days of incubation at 29 °C; scale bar = 30 μm (A, B) or 15 μm (A′, B′).
533 White arrows indicate border cell clusters. White lines indicate extent of migration of border cell
534 clusters, and red lines indicate extent of migration of main body cells. (C) Quantification of
535 border cell migration during stage 9 from control and Rux-expressing females after two days of
536 incubation at 29°C across five biological replicates. Each dot represents one egg chamber with
537 the distance migrated by its main body and border cells plotted on the x- and y-axis,
538 respectively. (D- E‴) DAPI staining and immunolabeling against FasIII and E-cadherin in
539 control (D-D‴) and Rux-expressing (E-E‴) border cell clusters after two days of incubation at
540 29 °C; scale bar = 10 μm.

541

Figure 1

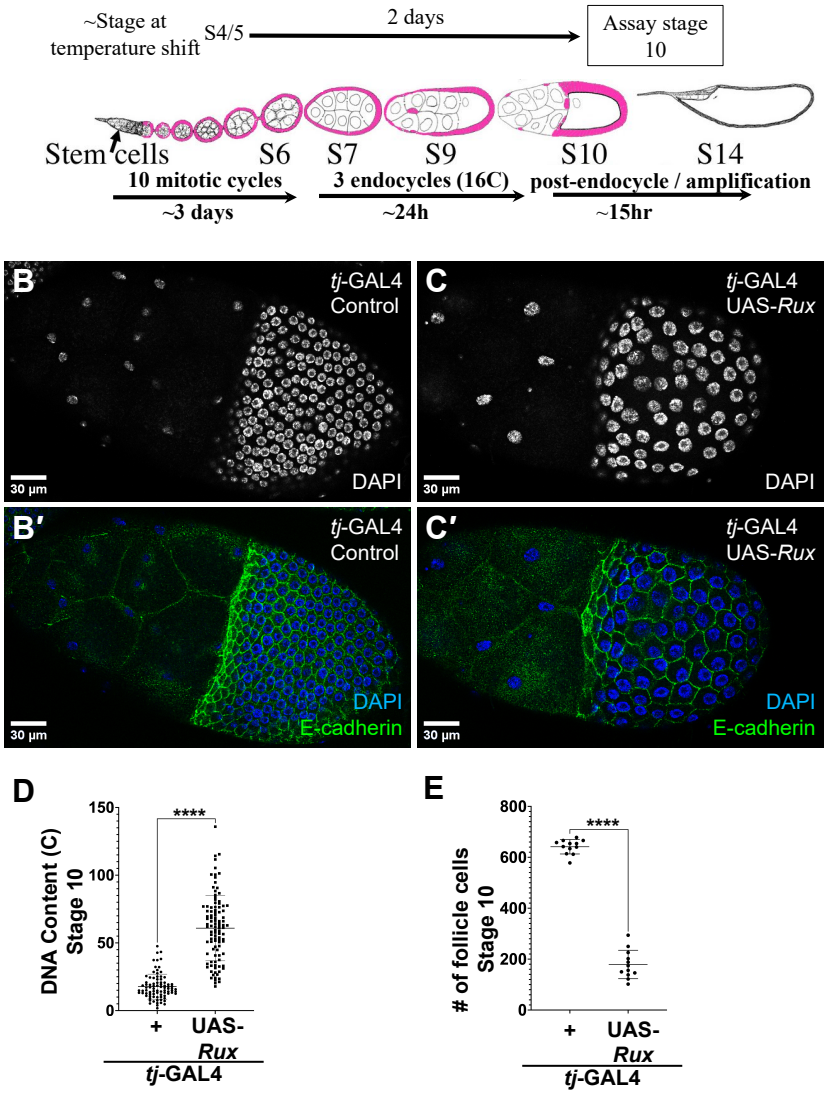
A
~Stage at temperature shift
S4/5
2 days
Assay stage 10
Stem cells
S6
S7
S9
S10
S14
10 mitotic cycles
~3 days
3 endocycles (16C)
~24h
post-endocycle / amplification
~15hr
B
tj-GAL4
Control
DAPI
30 µm
C
tj-GAL4
UAS-Rux
DAPI
30 µm
B′
tj-GAL4
Control
DAPI
E-cadherin
30 µm
C′
tj-GAL4
UAS-Rux
DAPI
E-cadherin
30 µm
D
DNA Content (C)
Stage 10
150
100
50
0
****
+
UAS-Rux
tj-GAL4
E
# of follicle cells
Stage 10
800
600
400
200
0
****
+
UAS-Rux
tj-GAL4

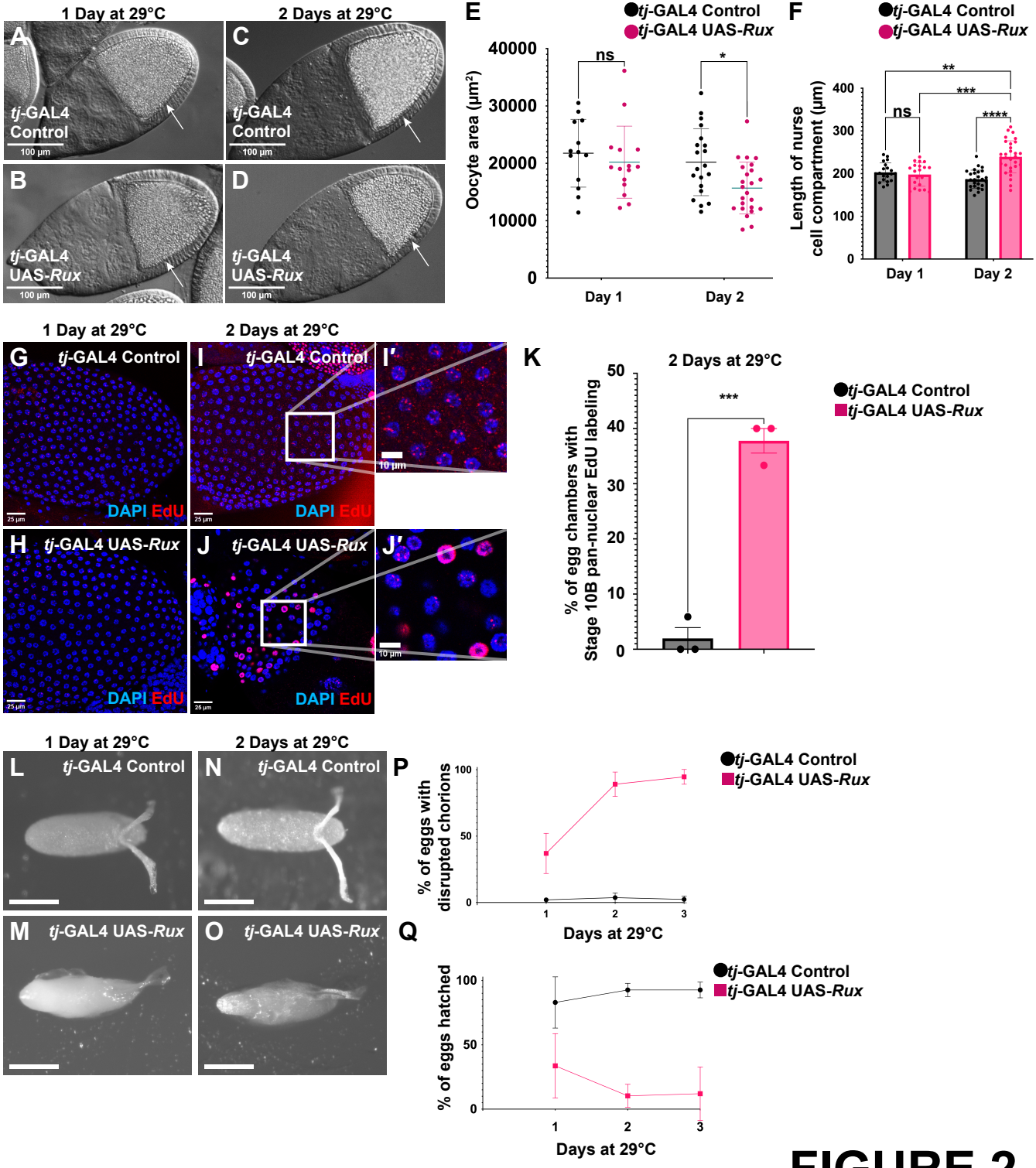
1 Day at 29°C
2 Days at 29°C
A
tj-GAL4 Control
100 µm
B
tj-GAL4 UAS-Rux
C
D
E
tj-GAL4 Control
tj-GAL4 UAS-Rux
Oocyte area (µm²)
ns
*
Day 1
Day 2
F
Length of nurse cell compartment (µm)
**
***
****
G
I
I'
H
J
J'
DAPI EdU
25 µm
10 µm
K
% of egg chambers with Stage 10B pan-nuclear EdU labeling
L
M
N
O
P
% of eggs with disrupted chorions
Days at 29°C
Q
% of eggs hatched

FIGURE 2

FIGURE 3

1 Day at 29°C

2 Days at 29°C

A *tj*-GAL4 Control
S2
S3/4
S5/6
S1
G
DAPI
15 µm

B *tj*-GAL4 UAS-*Rux*
S2
S3/4
DAPI
15 µm

C *tj*-GAL4 Control
S2
S3
S4
DAPI
15 µm

D *tj*-GAL4 UAS-*Rux*
S3/4
S5
DAPI
15 µm

A′ *tj*-GAL4 Control
S2
S3/4
S5/6
S1
G
E-cadherin
15 µm

B′ *tj*-GAL4 UAS-*Rux*
S2
S3/4
E-cadherin
15 µm

C′ *tj*-GAL4 Control
S2
S3
S4
E-cadherin
15 µm

D′ *tj*-GAL4 UAS-*Rux*
S3/4
S5
E-cadherin
15 µm

A″ *tj*-GAL4 Control
S2
S3/4
S5/6
S1
G
DAPI
E-cadherin
15 µm

B″ *tj*-GAL4 UAS-*Rux*
S2
S3/4
DAPI
E-cadherin
15 µm

C″ *tj*-GAL4 Control
S2
S3
S4
DAPI
E-cadherin
15 µm

D″ *tj*-GAL4 UAS-*Rux*
S3/4
S5
DAPI
E-cadherin
15 µm

E

2 Days at 29°C

DNA Content (C) Stage4/5

50
40
30
20
10
0

****

+

UAS-*Rux*

tj-GAL4

FIGURE 4

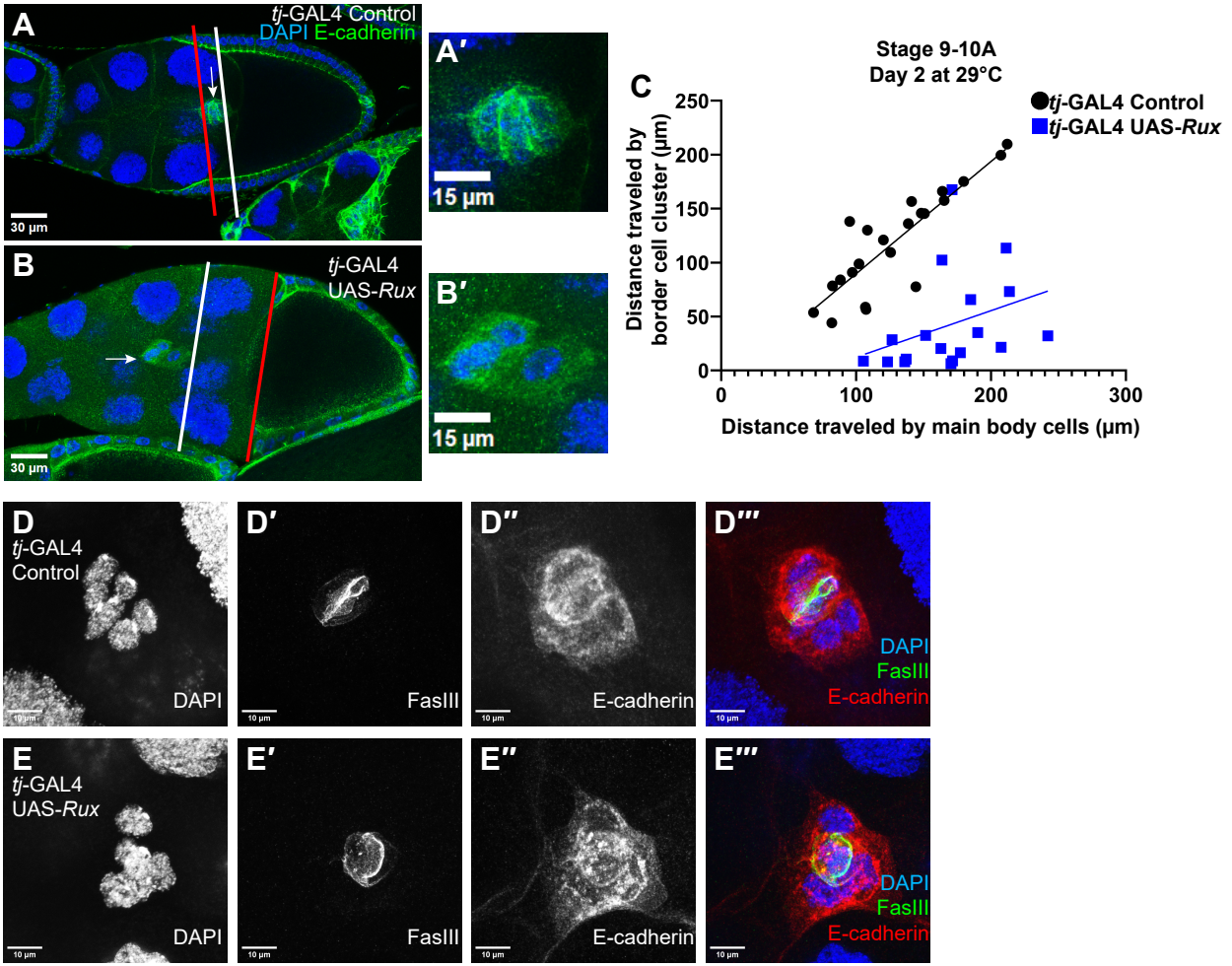
A
tj-GAL4 Control
DAPI E-cadherin
30 µm
A′
15 µm
B
tj-GAL4
UAS-Rux
30 µm
B′
15 µm
C
Stage 9-10A
Day 2 at 29°C
tj-GAL4 Control
tj-GAL4 UAS-Rux
Distance traveled by border cell cluster (µm)
Distance traveled by main body cells (µm)
0
50
100
150
200
250
0
100
200
300
D
tj-GAL4
Control
DAPI
D′
FasIII
D″
E-cadherin
D‴
DAPI
FasIII
E-cadherin
E
tj-GAL4
UAS-Rux
DAPI
E′
FasIII
E″
E-cadherin
E‴
DAPI
FasIII
E-cadherin